



**HAL**  
open science

# Ultrafast sunlight-induced polymerization: Unveiling 2phenylnaphtho[2,3-d]thiazole-4,9-dione as a unique scaffold for high-speed and precision 3D printing

Ji Feng, Yijun Zhang, Fabrice Morlet-Savary, Michael Schmitt, Jing Zhang, Pu Xiao, Frédéric Dumur, Jacques Lalevée

## ► To cite this version:

Ji Feng, Yijun Zhang, Fabrice Morlet-Savary, Michael Schmitt, Jing Zhang, et al.. Ultrafast sunlight-induced polymerization: Unveiling 2phenylnaphtho[2,3-d]thiazole-4,9-dione as a unique scaffold for high-speed and precision 3D printing. *Small*, 2024, 20 (32), pp.2400230. 10.1002/smll.202400230 . hal-04670097

**HAL Id: hal-04670097**

**<https://hal.science/hal-04670097>**

Submitted on 11 Aug 2024

**HAL** is a multi-disciplinary open access archive for the deposit and dissemination of scientific research documents, whether they are published or not. The documents may come from teaching and research institutions in France or abroad, or from public or private research centers.

L'archive ouverte pluridisciplinaire **HAL**, est destinée au dépôt et à la diffusion de documents scientifiques de niveau recherche, publiés ou non, émanant des établissements d'enseignement et de recherche français ou étrangers, des laboratoires publics ou privés.

1           **Ultrafast sunlight-induced polymerization: Unveiling 2-**  
2           **phenyl naphtho[2,3-*d*]thiazole-4,9-dione as a unique scaffold**  
3           **for high-speed and precision 3D printing**

4  
5           **Ji Feng <sup>a,b</sup>, Yijun Zhang <sup>a,b</sup>, Fabrice Morlet-Savary <sup>a,b</sup>, Michael Schmitt <sup>a,b</sup>, Jing**  
6           **Zhang <sup>c</sup>, Pu Xiao <sup>d\*</sup>, Frédéric Dumur <sup>e\*</sup>, and Jacques Lalevée <sup>a,b\*</sup>**

7  
8           <sup>a</sup> Université de Haute-Alsace, CNRS, IS2M UMR7361, F-68100 Mulhouse, France.

9   <sup>b</sup> Université de Strasbourg, France.

10           <sup>c</sup> Future Industries Institute, University of South Australia, Mawson Lakes, SA 5095,  
11   Australia.

12           <sup>d</sup> State Key Laboratory of High Performance Ceramics and Superfine Microstructure,  
13           Shanghai Institute of Ceramics, Chinese Academy of Sciences, Shanghai 200050, P.  
14   R. China.

15           <sup>e</sup> Aix Marseille Univ, CNRS, ICR, UMR 7273, F-13397 Marseille, France.

16  
17           E-mail address: jacques.lalevee@uha.fr (J. L.); frederic.dumur@univ-amu.fr (F.D.);

18   p.xiao@mail.sic.ac.cn (P.X.)

19  
20  
21  
22           **Abstract:** A series of 15 novel dyes based on the 2-phenyl naphtho[2,3-*d*]thiazole-4,9-  
23           dione scaffold and one compound based on the 2,3-diphenyl-1,2,3,4-  
24           tetrahydrobenzo[*g*]quinoxaline-5,10-dione scaffold are synthesized and studied as  
25           photoinitiators. These compounds are used in two- and three-component high-  
26           performance photoinitiating systems for the free radical polymerization of  
27           trimethylolpropane triacrylate (TMPTA) and polyethylene glycol diacrylate (PEGDA)  
28           under natural sunlight conditions. Remarkably, the conversion of TMPTA can reach  
29           ~60% within a mere 20 seconds, while PEGDA attains a 96% conversion within 90  
30           seconds. To delve into the intricate chemical mechanisms governing free radical  
31           polymerization, an array of analytical techniques is employed. Specifically, UV-visible  
32           absorption and fluorescence emission spectra, steady-state photolysis experiments,  
33           stability experiments, fluorescence quenching experiments, cyclic voltammetry, and

34 electron spin resonance spin trapping (ESR-ST) experiments, collectively contribute to  
35 a comprehensive understanding of the photochemical mechanisms. In addition, the  
36 photoinitiation capacities of these diverse systems are determined using Real Time  
37 Fourier Transformed Infrared Spectroscopy (RT-FTIR). Of particular interest is the  
38 revelation that, owing to the superior initiation ability of the various dyes, high-  
39 resolution 3D patterns can be successfully manufactured by direct laser write (DLW)  
40 technology and 3D printing. This underscores the efficient initiation of free radical  
41 polymerization processes by the newly developed dyes under both artificial and natural  
42 light sources, presenting an avenue for energy-saving and environmentally friendly  
43 polymerization conditions.

44

45 **Keywords:** Sunlight-induced polymerization; Naphthoquinone; photoinitiators; 2-  
46 Phenyl naphtho[2,3-*d*]thiazole-4,9-dione; 3D printing.

47

## 48 **1. Introduction**

49 In recent years, the application of photopolymerization has witnessed a significant  
50 expansion, both in industrial production and academic research. This surge can be  
51 attributed to the myriad advantages of photopolymerization, encompassing its  
52 environmentally friendly nature, absence of organic solvents, and safe operational  
53 conditions when employing visible light [1, 2]. With the evolution of LED technology,  
54 energy-efficient conditions have further become applicable to photopolymerization  
55 processes. The versatility of photopolymerization technology is exemplified in its  
56 applications, spanning 3D printing, biomedical materials development, coatings,  
57 dentistry, and various other applications [3-10].

58 Among the diverse photopolymerization techniques, free radical polymerization  
59 (FRP) stands out as one of the most prevalent and important technologies [11, 12],  
60 offering mild reaction conditions, high monomer conversions, and rapid polymerization  
61 rates. The efficacy of FRP processes is closely tied to the properties of the employed  
62 photoinitiators (PIs). Over the years, various photoinitiators have been explored to

63 enhance their performance across visible range. The pivotal factor in  
64 photopolymerization revolves around the ability of the photoinitiator/photosensitizer to  
65 efficiently interact with the light source [13, 14]. The initiation process hinges on the  
66 light absorption capacity of the photoinitiating systems that is governed by the molar  
67 extinction coefficients of the PIs. Additionally, the absorption maximum plays a crucial  
68 role in determining the excitation wavelength of a chromophore, influencing the  
69 efficacy of the electron or energy transfer from the photosensitizer to the different  
70 additives within the photocurable resin [15]. Up to now, common irradiation  
71 wavelengths have resided in the ultraviolet (UV) (< 400 nm) and UV-visible (405 nm,  
72 415 nm, etc.) range [16, 17]. However, the most optimal light source remains sunlight,  
73 presenting a renewable and free energy option for photopolymerization. Similar to  
74 photosynthesis in plants [15], direct photopolymerization under natural sunlight is now  
75 a focal point of intense research efforts.

76 Sunlight, as a rich and sustainable energy source, remains inexhaustible as long as  
77 the sun shines. Consequently, the development of sunlight-induced reactions holds a  
78 prominent position in contemporary [18], encompassing areas such as CO<sub>2</sub> conversion  
79 and decomposition [19, 20]. Another critical consideration in photopolymerization is  
80 the photoinitiator itself, posing challenges in the development of efficient  
81 photoinitiators suitable for sunlight-induced reactions [21]. Unlike artificial light  
82 sources, sunlight exhibits lower intensity than LEDs, accompanied by a much wider  
83 emission spectrum [22]. This distinction renders many photoinitiating systems, easily  
84 activated with LEDs, ineffective in initiating polymerization under sunlight [23]. Even  
85 in instances where polymerization can be initiated under sunlight, the process often  
86 extends over several hours, with reduced monomer conversions compared to LED-  
87 initiated polymerization [3]. Our previous research has identified many dyes with  
88 excellent photoinitiation performance when used in multicomponent systems[24, 25];  
89 however most of these were limited to LED activation. Thus, the development of dyes  
90 capable of efficiently initiating polymerization processes under sunlight assumes  
91 paramount significance.

92 This study introduced 15 dyes based on the 2-phenylnaphtho[2,3-*d*]thiazole-4,9-  
93 dione scaffold and 1 dye based on 2,3-diphenyl-1,2,3,4-  
94 tetrahydrobenzo[*g*]quinoxaline-5,10-dione, hitherto unreported in the literature. These  
95 dyes exhibited outstanding photoinitiation abilities under UV-visible light (e.g.  
96 LED@405 nm and LED@450 nm). Notably, five of the dyes exhibited the exceptional  
97 photoinitiating ability under sunlight, enabling rapid resin curing within one minute of  
98 exposure. The achieved monomer conversions, obtained at low photoinitiator/additive  
99 content and short exposure time (RT-FTIR profiles), represented an unprecedented  
100 advancement in the field. The elucidation of the photochemical mechanisms governing  
101 the polymerization process involved a comprehensive analysis of light absorption and  
102 fluorescence characteristics, cyclic voltammetry and ESR-ST experiments. The  
103 findings culminated in the successful application of several formulations exhibiting  
104 excellent photoinitiation abilities in DLW and 3D printing, yielding clear and precise  
105 3D patterns. Leveraging the remarkable performance in outdoor sunlight  
106 polymerization and applications in 3D printing, the dyes based on 2-  
107 phenylnaphtho[2,3-*d*]thiazole-4,9-dione scaffold have emerged as promising  
108 candidates for green polymer synthesis and large-scale outdoor applications.

## 109 **2. Experimental Process**

### 110 **2.1 Dyes and other materials.**

111 A collection of 16 dyes used for photopolymerization (under UV-visible light and  
112 under sunlight in the air) were successfully synthesized. Chemical structures are shown  
113 in Figure 1, and the synthetic routes used to prepare these compounds are detailed in  
114 the following Section 3.1 and in supporting information. The different monomers i.e.  
115 TMPTA and PEGDA (average  $M_n$  575g/mol) were all purchased from Sartomer  
116 (France). The benchmark commercial photoinitiator 2-isopropylthioxanthone (ITX)  
117 used for comparison was obtained from Sartomer-Lambson (United Kingdom). Ethyl  
118 4-dimethylaminobenzoate (EDB) used as the electron donor and *bis*(4-*tert*-  
119 butylphenyl)iodonium hexafluorophosphate (Iod) as the electron acceptor were  
120 purchased from Sartomer-Lambson (United Kingdom) (See Figure S1).

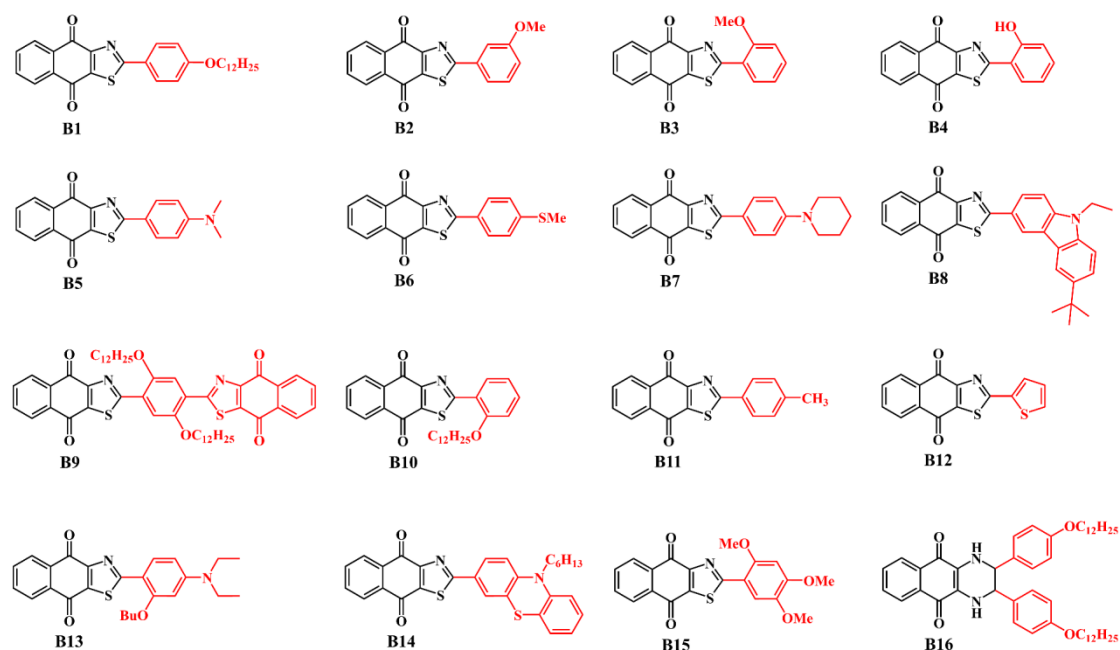


Figure 1. Chemical structures of dyes B1-B16.

## 2.2 UV-visible absorption and fluorescence properties of Dyes.

The UV-visible absorption properties and UV steady-state photolysis of the sixteen dyes, dissolved in dichloromethane at a concentration of  $5 \times 10^{-5}$  M, were studied using a JASCO V730 spectrophotometer. Steady-state photolysis of the different systems (dye, dye/EDB, dye/Iod, dye/EDB/Iod) were investigated upon irradiation (e.g. under LED@405 nm). Maintaining the consistent dye concentration in dichloromethane, fluorescence spectra of the different dyes were measured using the JASCO FP-6200 fluorescence spectrophotometer, and the fluorescence excited state lifetimes were determined using the HORIBA PPD-850 fluorimeter.

Fluorescence quenching experiments were performed using the JASCO FP-6200 spectrofluorometer, allowing for the extraction of pertinent of parameters such as the electron transfer quantum yields ( $\phi_{et}$ ) using equation (1). The Stern-Volmer coefficients ( $K_{sv}$ ) correspond to the slopes of the Stern-Volmer treatment in the fluorescence quenching experiments.

$$\phi_{et} = \frac{K_{sv}[\text{additive}]}{1+K_{sv}[\text{additive}]} \quad (1)$$

140

### 141 **2.3 Free radical photopolymerization (FRP) under near UV/visible-light** 142 **irradiation and sunlight-induced polymerization under air.**

143 The different formulations used for photopolymerization were prepared as follows:  
144 dye/EDB (two-component) and dye/EDB/Iod (three-component) were mixed and  
145 dissolved into TMPTA, and then stirred overnight in the dark. The weight content of  
146 dye, EDB and Iod were calculated based on the weight of the monomer, and the  
147 influence of the different weight content ratio of each component on the  
148 photopolymerization efficiency were investigated. After that, the prepared formulations  
149 were subjected to photopolymerization experiments of thick and thin samples, and the  
150 specific operations were as follows: one drop of the prepared resin was dropped  
151 between two polypropylene films (for thickness from 10 to 100 microns) for thin  
152 samples, and five drops of the prepared resins were dropped into a plastic mold (2 mm)  
153 for thick samples. Then, the characteristic peaks of acrylate functional groups were  
154 continuously detected at about  $6150\text{ cm}^{-1}$  (2 mm thick sample) and  $1650\text{ cm}^{-1}$  (thin  
155 sample 10 to 100 microns) by RT-FTIR (JASCO FTIR-4700). The acrylate conversions  
156 were obtained by the following equation:

$$157 \text{ Conversion (\%)} = \left(1 - \frac{A_t}{A_0}\right) \times 100\% \quad (2)$$

158 where  $A_0$  is the initial peak area before light irradiation and  $A_t$  is the peak area  
159 after being irradiated with light for  $t$  s.

160 In addition to the polymerization experiments conducted under artificial light  
161 sources, we explored sunlight-induced photopolymerization using the same  
162 formulations as described earlier. The sunlight-induced polymerization experiment was  
163 carried out on August 22, 2023, from 1 pm to 3 pm, aligning with French time. The  
164 experiment site was in Mulhouse (+77 43 ' E, 47 75 ' N), France, where the weather  
165 conditions were sunny. The conversions of the acrylate functional groups were  
166 monitored by RT-FTIR spectroscopy.

### 167 **2.4 Redox potentials of dyes obtained by cyclic voltammetry.**

168 Redox potentials of the dyes were measured using cyclic voltammetry. The

169 specific operation was that the dyes and the supporting electrolyte  
170 (tetrabutylammonium hexafluorophosphate) were dissolved in dichloromethane, and  
171 the redox potentials of the dyes were measured under nitrogen atmosphere. Equations  
172 (3) and (4) were used to calculate the change of free energy ( $\Delta G^{S^1}_{EDB}$  or  $\Delta G^{S^1}_{Iod}$ ) from  
173 the excited singlet states in the electron transfer reaction between the dyes and the  
174 additives. The singlet excited state energy level ( $E_{S^1}$ ) of the dyes was determined from  
175 the intersection of the normalized UV-visible absorption and fluorescence spectra.  
176 Finally, the oxidation potential of EDB is 1.0 V and the reduction potential of the  
177 iodonium salt (Iod) is -0.7 V, as reported in the literature [26, 27].

178

$$179 \Delta G^{S^1}_{Iod} = E_{ox} - (-0.7) - E_{S^1} \quad (3)$$

$$180 \Delta G^{S^1}_{EDB} = 1 - E_{red} - E_{S^1} \quad (4)$$

181

## 182 **2.5 Electron Spin Resonance – Spin Trapping (ESR-ST) experiments.**

183 ESR-ST experiments were carried out with the ESR X-band spectrometer (Bruker  
184 EMX-plus) to study the free radicals generated under the LED@405 nm irradiation.  
185 Under nitrogen atmosphere, free radicals were captured by phenyl-*N-tert*-butylnitrone  
186 (PBN). The concentration of PBN was  $\sim 5 \times 10^{-4}$  M. All operations were carried out at  
187 room temperature. In addition, ESR-ST spectra were simulated by PEST WINSIM  
188 program.

## 189 **2.6 Application of 3D printing experiments.**

190 The formulations with good photopolymerization performance were selected for  
191 3D printing experiments. First of all, a two-component system (0.1wt% dye/1wt% EDB,  
192 TMPTA as the monomer) was used to conduct the direct laser write (DLW) experiments  
193 with a computer-programmed x,y desk with a mounted laser diode at 405 nm, in which  
194 the glass tank (3 cm in length, 2 cm in width, and 0.3 cm in height) for printing was  
195 made by ourselves. Furthermore, a three-component system (0.1wt% dye/1wt%  
196 EDB/1wt% Iod, TMPTA as the monomer) was used to print 3D objects with a Digital  
197 Light Processing (DLP) 3D Printer (Anycubic Photon D2, China), and the thickness of  
198 the layer was controlled at 0.02 mm. The printed patterns were observed by Scanning

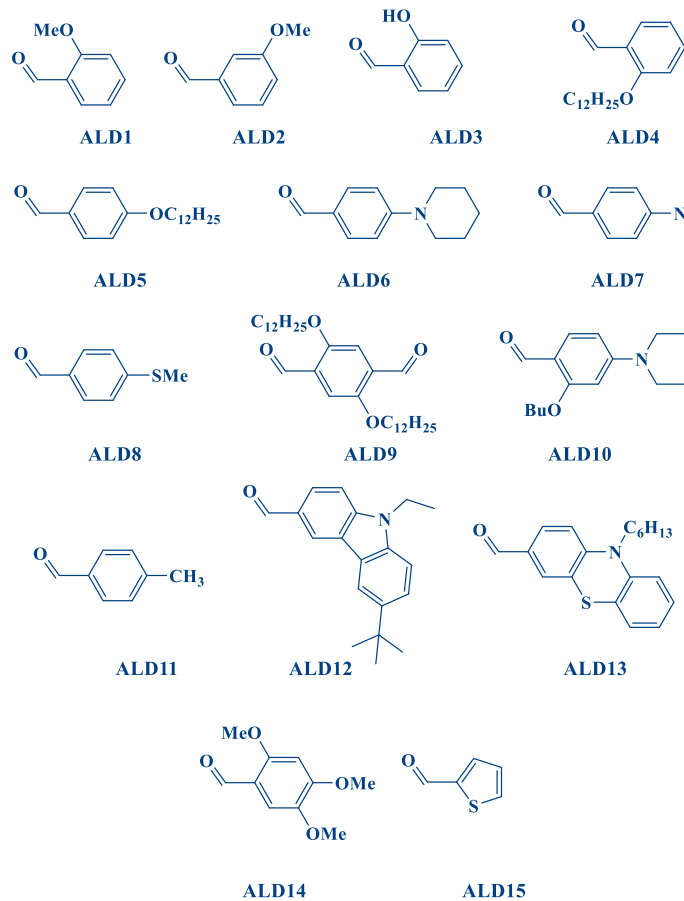
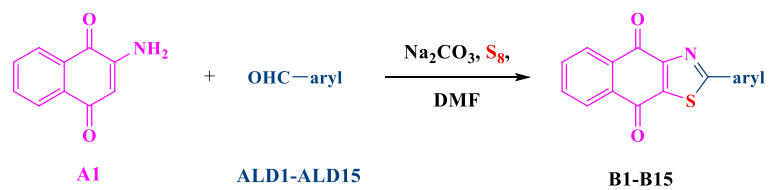


199 Electron Microscope (SEM) and Numerical Optical Microscope (DSX-HRSU from  
200 Olympus Corporation).

### 201 **3. Results and Discussion**

#### 202 **3.1 Synthesis of the dyes.**

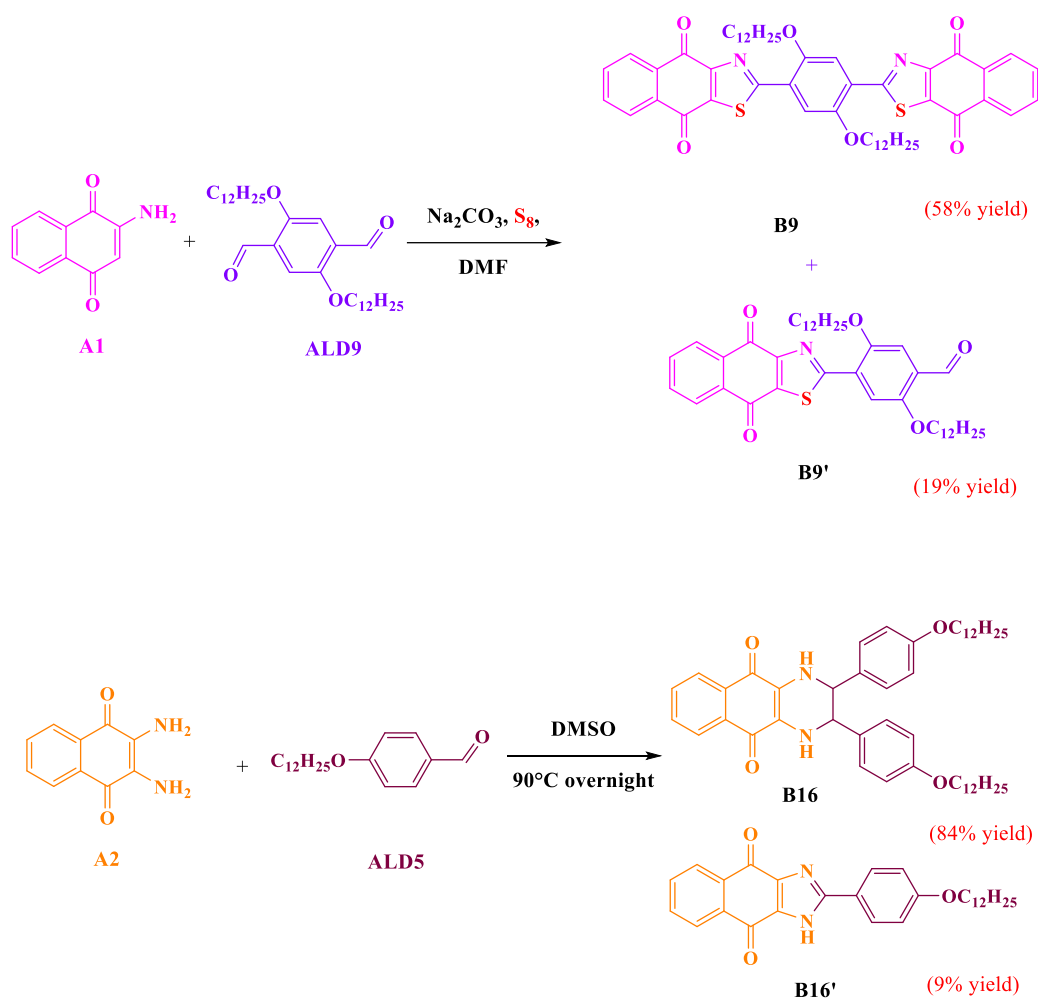
203 B1-B15 were prepared in one step starting from 2-aminonaphthalene-1,4-dione A1  
204 and the appropriate aldehyde ALD1-ALD15 using the synthetic route as reported  
205 previously [28] (See Scheme 1). With this method, all dyes could be obtained with the  
206 reaction yields ranging between 58% yield for B9 and 92% yield for B10 after  
207 purification/isolation (See Table 1). It has to be noticed that all dyes exhibited a D- $\pi$ -A  
208 structure (with D and A standing for donor and acceptor respectively) except for B9 that  
209 A- $\pi$ -D- $\pi$ -A was found. To access to this structure, 2,5-  
210 *bis*(dodecyloxy)terephthalaldehyde ALD9 was used as the dialdehyde (See Scheme 2).  
211 Among the series of dyes, the lowest reaction yield (58%) was obtained during the  
212 synthesis of this dye, 4-(4,9-dioxo-4,9-dihydronaphtho[2,3-*d*]thiazol-2-yl)-2,5-  
213 *bis*(dodecyloxy)benzaldehyde B9' being isolated as the side product of this reaction in  
214 19% yield. A different synthesis was used for B16. Starting from 2,3-  
215 diamionaphthalene-1,4-dione A2 and two equivalents of 4-(dodecyloxy)benzaldehyde,  
216 B16 could be identified as the main product of the reaction and isolated in 84% yield.  
217 As a side product of this second reaction, 2-(4-(dodecyloxy)phenyl)-1*H*-naphtho[2,3-  
218 *d*]imidazole-4,9-dione B16' could be obtained in 9% yield (See Scheme 2). It has to be  
219 noticed that the synthetic route used to produce B16 was first reported in 1987 and the  
220 synthesis of such compounds has never been revisited since this pioneering work [29].



221

222

**Scheme 1.** Synthetic routes to B1-B15.



223

224

**Scheme 2.** Synthetic routes to B9 and B16.

225

226

**Table 1.** Reaction total yields obtained during the synthesis of B1-B16.

Compounds	Reaction yields (%)	Compounds	Reaction yields (%)
B1	81	B9	58
B2	77	B10	92
B3	89	B11	81
B4	80	B12	88
B5	67	B13	65
B6	88	B14	85
B7	88	B15	85
B8	91	B16	84

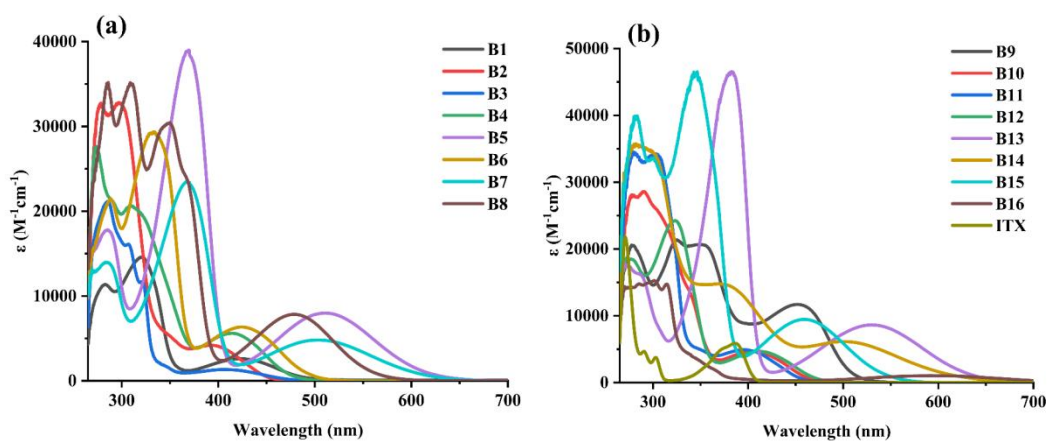
227

### 228 3.2 Light absorption properties of the different dyes.

229 UV-visible absorption spectra of the 16 dyes and the commercial photoinitiator 2-

230 isopropylthioxanthone (ITX) dissolved in dichloromethane were recorded and the

231 results are shown in Figure 2. Light absorption characteristics of the different dyes are  
 232 summarized in Table 2. Figure 2 vividly illustrates robust absorption peaks in the UV-  
 233 visible region for all dyes, assigned to  $\pi \rightarrow \pi^*$  transitions [30]. Notably, the maximum  
 234 absorption peaks of B1, B2, B3, B4, B10, B11, and B12 were around 405 nm, which  
 235 were therefore highly favorable for photopolymerization experiments conducted under  
 236 the LED@405 nm and a benchmark in 3D printing (See Section 3.3). The maximum  
 237 absorption wavelengths ( $\lambda_{\max}$ ) of B1, B2, B3, B10, and B11 were 420, 400, 410, 410,  
 238 and 400 nm, respectively. Correspondingly, their molar extinction coefficients ( $\epsilon_{\max}$ ) at  
 239  $\lambda_{\max}$  were 2610, 4170, 1320, 4690, and 4920  $\text{M}^{-1} \cdot \text{cm}^{-1}$ , respectively. In addition, the  
 240 molar extinction coefficients ( $\epsilon_{405\text{nm}}$ ) at  $\lambda_{405\text{nm}}$  were 2310, 3870, 1320, 4690, and 4730  
 241  $\text{M}^{-1} \cdot \text{cm}^{-1}$ , respectively. These five dyes demonstrated excellent photoinitiation abilities,  
 242 and the results presented in Section 3.3 also confirmed their high photoinitiation  
 243 performance as photoinitiators in free radical polymerization when 2 mm thick resin  
 244 samples in open molds (no protection against oxygen inhibition) were exposed to  
 245 sunlight outdoors (clear sky conditions). Contrastingly, B5, B7-B9, and B13-B16  
 246 showed strong absorption peaks in the 450-600 nm range, which may be due to a  
 247 redshift of the  $\pi \rightarrow \pi^*$  transition with an increase of the electronic density, resulting from  
 248 the presence of strong electron-donating groups. However, these dyes exhibited poor  
 249 photoinitiation abilities [30], as elaborated in Section 3.3.



250  
 251 **Figure 2.** UV-visible absorption spectra of dyes in dichloromethane. (a) B1-B8, (b)  
 252 B9-B16 and ITX.  
 253

254 **Table 2.** Light absorption characteristics of the dyes ( $\lambda_{\max}$  for the red shifted  
 255 transitions)

PIs	$\lambda_{\max}$ (nm)	$\epsilon_{\max}$ ( $M^{-1}.cm^{-1}$ )	$\epsilon_{405}$ ( $M^{-1}.cm^{-1}$ )	moiety
B1	420	2610	2310	4-dodecyloxyphenyl
B2	400	4170	3870	3-methoxyphenyl
B3	410	1320	1320	2-methoxyphenyl
B4	410	5600	5410	2-hydroxyphenyl
B5	510	7990	4110	4-dimethylaminophenyl
B6	430	6340	5630	4-methylthiophenyl
B7	510	4810	4570	4-piperidinylphenyl
B8	480	7830	2400	<i>tert</i> -butyl-( <i>N</i> -ethyl)carbazolyl
B9	450	11690	8760	naphthothiazolodione- <i>bis</i> (dodecyloxy)phenylene
B10	410	4690	4690	2-dodecyloxyphenyl
B11	400	4920	4730	<i>p</i> -tolyl
B12	410	4660	4570	thiophenyl
B13	530	8630	12120	2-butoxy-4-(diethylamino)phenyl
B14	500	6130	11240	<i>N</i> -hexyl-phenothiazinyl
B15	460	9460	4530	2,4,5-trimethoxyphenyl
B16	590	1220	420	<i>bis</i> ( <i>p</i> -dodecyloxy)phenyl
ITX	390	5890	1000	

256

257 **3.3 Photopolymerization kinetics with the dyes in two or three-component**  
 258 **photoinitiating systems under LED@405 nm, 450 nm, and sunlight.**

259 To investigate the photoinitiation ability of the fifteen dyes based on the 2-  
 260 phenyl-naphtho[2,3-*d*]thiazole-4,9-dione scaffold and the one dye based on the 2,3-  
 261 diphenyl-1,2,3,4-tetrahydrobenzo[*g*]quinoxaline-5,10-dione scaffold,  
 262 photopolymerization were carried out under LED@405 nm, LED@450 nm, and  
 263 sunlight exposure. The photoinitiation ability of two different two-component  
 264 (dye/EDB and dye/Iod) systems and one three-component (dye/EDB/Iod) system were  
 265 studied to clarify the influence of co-initiators (EDB as the electron/hydrogen donor and  
 266 Iod as the electron acceptor) on the polymerization kinetics of TMPTA. The  
 267 conversions of acrylate functional groups were determined using the RT-FTIR at room  
 268 temperature. Specifically, for the blank groups shown in Figure S2 (i.e. dye alone, EDB  
 269 alone, and Iod alone), no polymerization or poor photoinitiation abilities were  
 270 determined, evidencing that the two co-initiators EDB and Iod may only play a crucial  
 271 role in the initiation step once combined with the dyes.

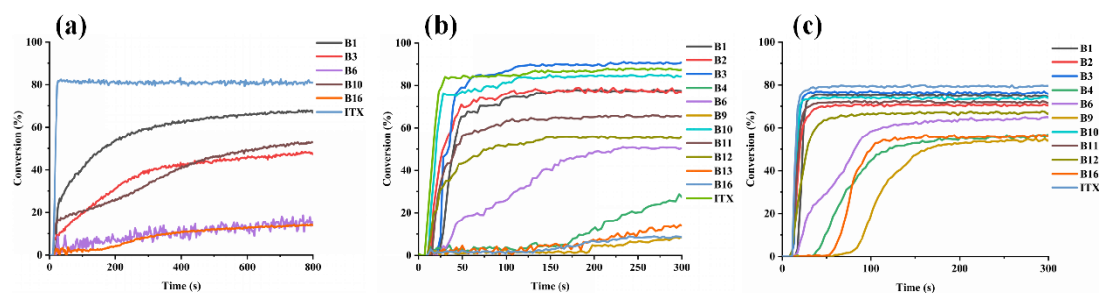
272 Polymerization profiles obtained with the two-component dye/EDB systems are

273 shown in Figure S3 (thick sample) and Figure S4 (thin sample), while the final acrylate  
274 function conversions (FCs) are listed in Table S1 (thick sample) and Table S2 (thin  
275 sample). Influence of the dye concentrations on the polymerization performance of  
276 TMPTA was also investigated. Specifically, for the two-component dye/EDB system,  
277 EDB concentration was fixed to 1 wt%. When the dye concentration was set to 0.1 wt%,  
278 the conversions of thick samples (See Figure S3(c)) and thin samples (See Figure S4(c))  
279 were optimal, especially for thick samples containing B1 and B10 and thin sample  
280 containing B16. The conversions of thick samples were close to 80%, while it can reach  
281 90% for the thin samples. It implied that when the dye concentrations were 1 wt%, the  
282 solubility of the dyes in TMPTA was low and the precipitation can be clearly seen in  
283 the different formulations, which led to a poor light penetration i.e. inner filter effect  
284 due to the high light absorption properties of the dyes. By decreasing the dye  
285 concentrations, the different formulations became clearer and more transparent, which  
286 can be beneficial to photopolymerization.

287 In the case of the two-component dye/Iod (1 wt%) system (See Figure S5 (thin  
288 sample) and Figure S6 (thick sample)), the results were basically consistent with that  
289 obtained with the two-component dye/EDB system. Considering that numerous dyes  
290 exhibited good light absorption properties in the 450-550 nm range, polymerization  
291 experiments were also carried out under the LED@450 nm, using the two-component  
292 dye/EDB (0.1%/1% w/w) system in TMPTA, both in thick and thin samples. Excellent  
293 polymerization performance could be determined, as shown in Figure S7.

294 Considering that the different dyes can form photoinitiating systems with Iod and  
295 EDB, their combination in three-component dye/Iod/EDB systems was also  
296 investigated. As shown in Figures 3 (a) and (b), in thick samples, when the  
297 concentration of EDB and Iod in TMPTA were kept constant at 1 wt%, the dye  
298 concentration of 0.1wt% furnished excellent polymerization profiles (See Figure 3 (b)).  
299 The FC with B3 even reached 91%, and the conversions with B10 and B1 were around  
300 80%. However, when the concentration of dyes was set to 1 wt%, the dyes were not  
301 completely dissolved in TMPTA, resulting in low polymerization efficiency (again

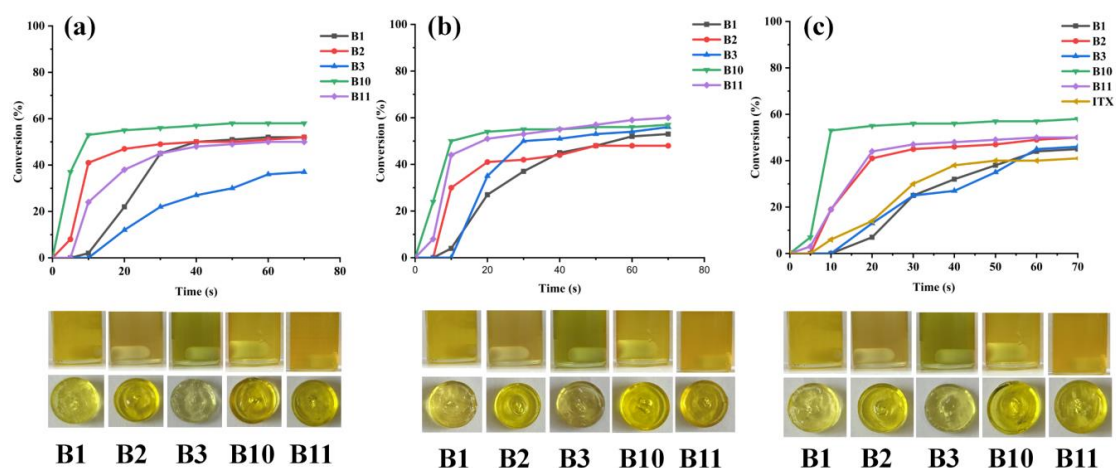
302 ascribed by an inner filter effect due to the high light absorption properties of the dyes).  
 303 When the amount of EDB and Iod were reduced to 0.1 wt% (See Figure 3 (c)), the  
 304 different three-component photoinitiating systems could maintain a high conversion  
 305 level and all thick samples could be deeply cured (See Figure S8 and Figure S9). In the  
 306 case of thin samples (See Figure S10), the higher conversions could be determined.  
 307 Specifically, polymerization of TMPTA initiated with the photoinitiating systems based  
 308 on B1, B2, B3, B10, and B11 was very fast, and the maximum monomer conversion  
 309 could be obtained within only 20 seconds of irradiation with LED@405nm and  
 310 LED@450 nm. On the contrary, other photoinitiating systems only showed poor  
 311 photoinitiation abilities, which was characterized by low conversions obtained after a  
 312 long induction period. As a result, B1, B2, B3, B10, and B11 were selected as the  
 313 photoinitiators/photosensitizers for photopolymerization experiments done under  
 314 sunlight and under air.



315  
 316 **Figure 3.** Photopolymerization profiles of TMPTA for thick sample (2 mm) upon  
 317 exposure to LED@405 nm irradiation. Initiated by (a) dye/EDB/Iod 1%/1%/1% w/w/w;  
 318 (b) dye/EDB/Iod 0.1%/1%/1% w/w/w; (c) dye/EDB/Iod 0.1%/0.1%/0.1% w/w/w. The  
 319 irradiation starts at  $t = 10$  s.

320 The sunlight-induced photopolymerization were carried out at 1-4 pm on August  
 321 22, 2023 in Mulhouse, France. As shown in Figure 4, three kinds of two-component  
 322 and three-component systems with excellent photoinitiation abilities under artificial  
 323 irradiation were selected to for the photopolymerization under sunlight (thick sample,  
 324 2 mm). Interestingly, the three systems showed high performance under sunlight.  
 325 Photopolymerization profiles obtained with the two-component (dye/EDB 0.1%/1%  
 326 w/w) system are shown in Figure 4 (a), while those of the three-component systems are

327 presented in Figures 4 (b) and (c). All FCs are listed in Table 3. It can be seen from the  
 328 three-component systems that B10 reached the over 50% functional conversion (green  
 329 curve) within 10 s and compared to the other four dyes, even for the system with the  
 330 low concentrations of additives (i.e., dye/EDB/Iod 0.1%/0.1%/0.1% w/w/w; Figure 4  
 331 (c)). Change of the formulations before and after polymerization is also given at the  
 332 bottom of Figure 4 and according to the experimental results, there were still a little  
 333 liquid at the surface of the resins containing B1 and B2 after polymerization, but for  
 334 resins containing B3, B10, B11, and ITX, they were completely polymerized as solids  
 335 (tack-free surfaces). It can be seen that all thick samples could be deeply cured with  
 336 sunlight. Based on the excellent polymerization performance of these dyes under  
 337 sunlight, polymerization experiments were also carried out with the three-component  
 338 (dye/EDB/Iod 0.1%/1%/1% w/w/w) system in another monomer PEGDA. As shown in  
 339 Figure S11, the acrylate functional group conversion of PEGDA initiated by B10  
 340 reached 96%, which was similar to that of the commercial initiator ITX. According to  
 341 the above experimental results, B10 synthesized in this study has a great application  
 342 prospect in inducing photopolymerization under sunlight.



343  
 344 **Figure 4.** Photopolymerization profiles of TMPTA for thick sample (2 mm) under  
 345 sunlight in the air. Initiated by (a) dye/EDB 0.1%/1% w/w; (b) dye/EDB/Iod 0.1%/1%/1%  
 346 w/w/w; (c) dye/EDB/Iod 0.1%/0.1%/0.1% w/w/w. (Black curve for B1, red curve for  
 347 B2, blue curve for B3, green curve for B10, purple curve for B11 and yellow curve for  
 348 ITX)



349

350 **Table 3.** Final acrylate function conversions (FCs) of TMPTA in the presence of dyes  
 351 with co-initiators under sunlight-induced polymerization.

<b>Two-component</b>		<b>Three-component</b>		<b>Three-component</b>	
<b>Dye/EDB</b>		<b>Dye/EDB/Iod</b>		<b>Dye/EDB/Iod</b>	
<b>(0.1%/1% w/w)</b>		<b>(0.1%/1%/1%)</b>		<b>(0.1%/0.1%/1%)</b>	
<b>Monomer: TMPTA</b>		<b>Monomer: TMPTA</b>		<b>Monomer: TMPTA</b>	
Dye	FCs (%)	Dye	FCs (%)	Dye	FCs (%)
B1	52	B1	53	B1	45
B2	52	B2	48	B2	50
B3	37	B3	56	B3	46
B10	58	B10	58	B10	58
B11	50	B11	61	B11	50

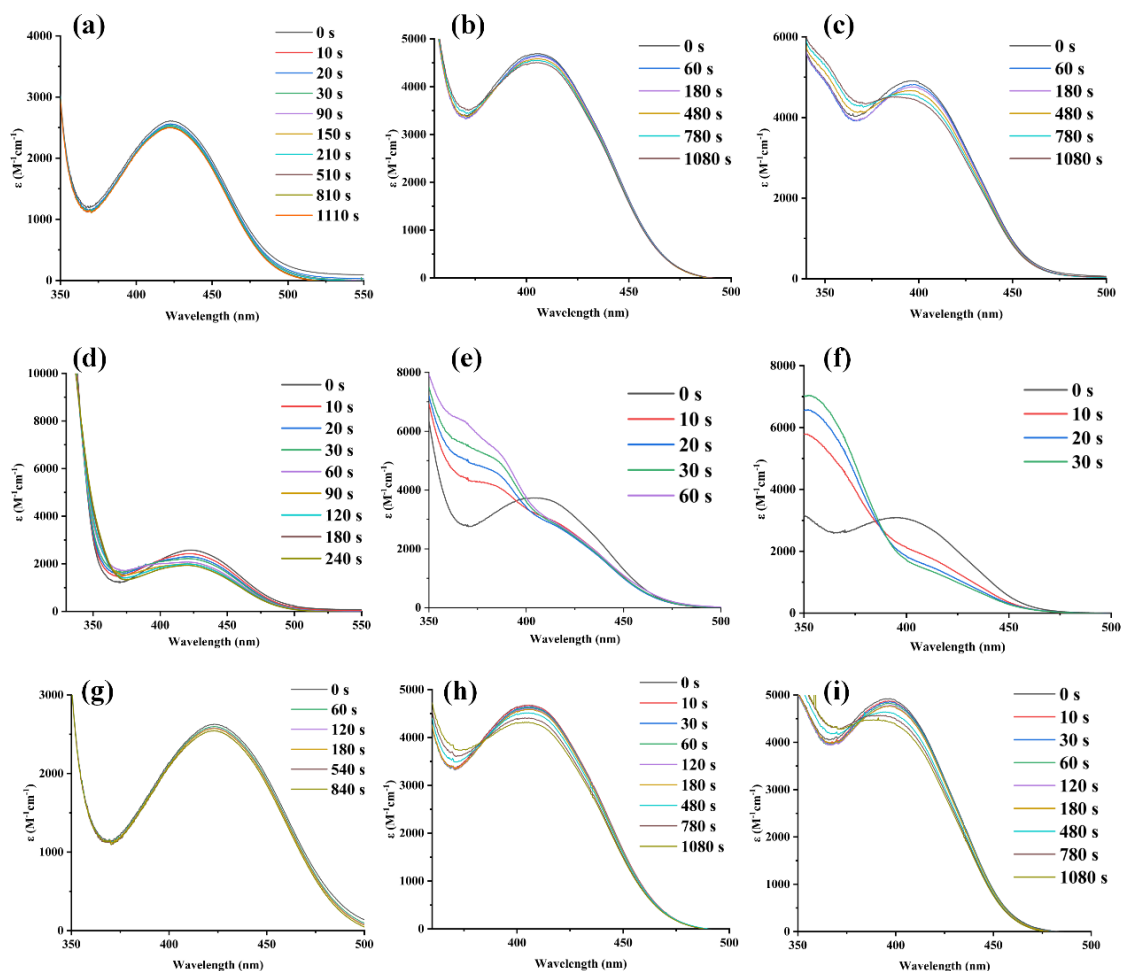
352

353 **3.4 Steady state photolysis experiments of dye, dye/EDB and dye/Iod**  
 354 **photoinitiation systems.**

355 To understand the interaction between the different dyes, EDB, and Iod, and to  
 356 clarify the chemical mechanism involved in the photopolymerization process, steady-  
 357 state photolysis experiments were carried out under the irradiation of LED@405 nm.  
 358 As shown in Figure 5, the UV-visible absorption profiles of dye, dye/EDB, and dye/Iod  
 359 dissolved in dichloromethane were studied respectively. The concentration was set as  
 360  $5 \times 10^{-5}$  M for dye,  $1 \times 10^{-4}$  M for EDB, and  $1 \times 10^{-4}$  M for Iod. All the steady-state  
 361 photolysis profiles are shown in Figures S12, S13 and S14.

362 As shown in Figures 5 (a), (b), and (c), the steady-state photolysis profiles of B1,  
 363 B10 and B11 are presented after 18 min of irradiation with the LED@405 nm.  
 364 Absorbance of the three dyes decreased slightly by elongating the irradiation time,  
 365 indicating that the dyes alone were relatively stable upon the irradiation with the  
 366 LED@405nm, which was in line with the photopolymerization results presented in  
 367 Section 3.3. Notably, the dyes alone cannot initiate any polymerization, or the monomer  
 368 conversion was low. However, in the case of the two-component dye/EDB systems, as  
 369 shown in Figure 5 (d), it can be seen that the absorbance of the B1/EDB system  
 370 obviously decreased within 4 min compared with the single dye system. In the case of

371 the B10/EDB system in Figure 5 (e) and B11/EDB system in Figure 5 (f), these  
 372 photolysis of two two-component systems were significant within only 30 s.  
 373 Interestingly, for the three two-component dye/Iod systems presented in Figures 5 (g),  
 374 (h), and (i), after a long period of irradiation, the absorbance was almost the same than  
 375 that of the single dye system. Obviously, the efficiency of dye/EDB combination was  
 376 higher than that of dye/Iod in the photopolymerization process.



377

378 **Figure 5.** Steady-state photolysis of dye ( $5 \times 10^{-5}$  M), EDB ( $1 \times 10^{-4}$  M) and Iod ( $1 \times 10^{-4}$   
 379 M) in dichloromethane under LED@405 nm. (a) dye-B1 (alone), (b) dye-B10 (alone),  
 380 (c) dye-B11 (alone), (d) dye-B1 and EDB, (e) dye-B10 and EDB, (f) dye-B11 and EDB,  
 381 (g) dye-B1 and Iod, (h) dye-B10 and Iod, (i) dye-B11 and Iod.

382

383 In addition, to test the stability of dyes under sunlight, steady-state photolysis  
 384 experiments of B1, B2, B3, B10 and B11 were also carried out under sunlight and under

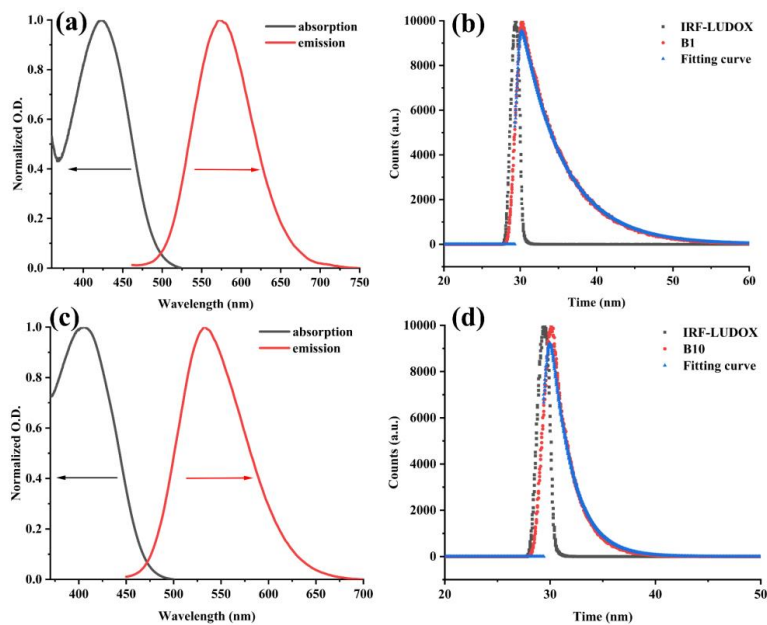
385 air. As shown in Figure S15, after a long-term sunlight irradiation, the absorbance  
386 hardly changed, which proved that the dyes had a good stability under sunlight. This  
387 also provides a basis for the practical application of these dyes.

### 388 **3.5 Fluorescence properties, fluorescence quenching experiments and chemical** 389 **mechanisms in electron transfer reaction for dyes.**

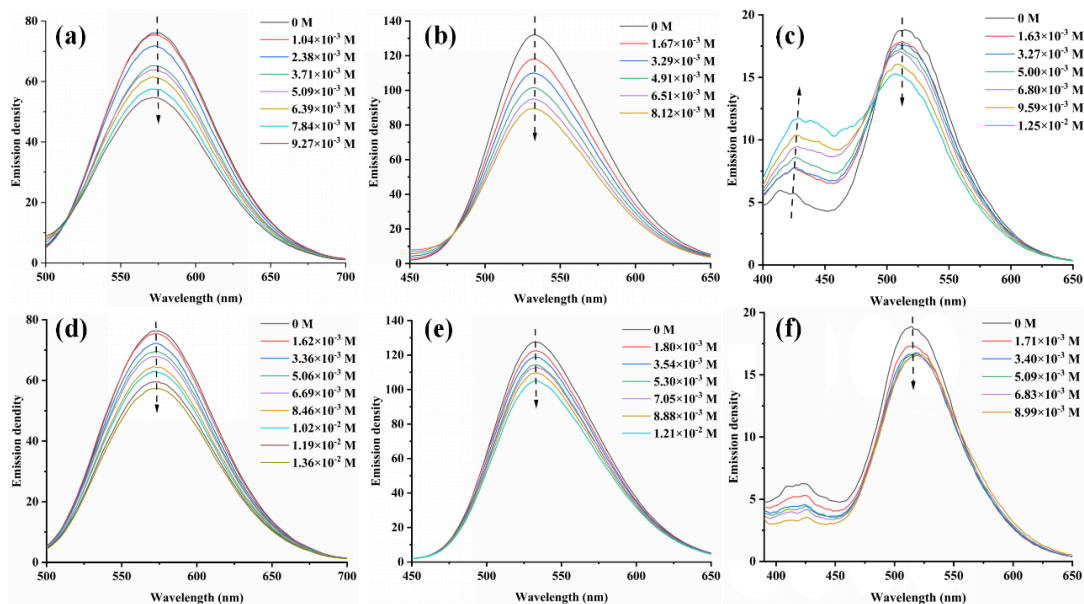
390 Fluorescence spectra of the different dyes are shown in Figure S16, and the  
391 fluorescence lifetime spectra are shown in Figures 6 and S17. Fluorescence  
392 characteristics of some dyes were not detected in the 200-1000 nm range due to their  
393 chemical structures. Various parameters in electron transfer reaction, such as  $E_{S1}$  (See  
394 Figures 6, S18 and Table 4), were obtained from the intersection of the normalized UV-  
395 visible absorption and fluorescence spectra. In addition, the oxidation ( $E_{ox}$ ) and  
396 reduction ( $E_{red}$ ) potentials of B1, B3, B10, B12, and B16 were measured by cyclic  
397 voltammetry (See Figure S19), and the values of  $E_{ox}$  and  $E_{red}$  are summarized in Table  
398 4. From Figure S19, the reduction peaks were clearly observed for the five investigated  
399 dyes, and the oxidation peaks were only observed for B3 and B16 during the sweep  
400 cycle. The Gibbs free energy change ( $\Delta G^{S1}$ ) of electron transfer between dyes and  
401 additives (EDB and Iod) were calculated according to equations (3) and (4), and the  
402 values are listed in Table 4. It can be seen from the Table that  $\Delta G^{S1}$  of all dyes were  
403 negative, indicating that the electron transfer reactions of dye/EDB and dye/Iod were  
404 feasible.

405 Fluorescence quenching experiments of the dye/EDB systems and the dye/Iod  
406 systems were also carried out in dichloromethane, as shown in Figure 7 and Figures  
407 S20 and S21. For B1, B10, and B11, the addition of additives (EDB and Iod)  
408 significantly decreased their fluorescence intensity. Conversely, the fluorescence  
409 intensity of B11/EDB increased at 400-450 nm, which may be due to the fact that dye-  
410 B11 reacted with EDB upon irradiation to generate new chromogenic substances, which  
411 indicated that there was an efficient interaction between the dyes and EDB or Iod. The  
412 results were consistent with the above free energy changes and steady-state photolysis  
413 experiments.

414 The Stern-Volmer coefficients ( $K_{sv}$ ) of dye/EDB or dye/Iod were determined by  
 415 the slope of the Stern–Volmer treatment of fluorescence quenching (See Figure S22),  
 416 and the electron transfer quantum yields ( $\phi_{et}$ ) (See Table 4) can be calculated by  
 417 Equation 1, which was helpful for a deep understanding of the chemical mechanism in  
 418 photopolymerization.



419  
 420 **Figure 6.** (a) Singlet state energy of B1, (b) fluorescence decay curve of B1, (c)  
 421 singlet state energy of B10, (d) fluorescence decay curve of B10.



422  
 423 **Figure 7.** Fluorescence quenching of (a) dye-B1 and EDB, (b) dye-B10 and EDB, (c)  
 424 dye-B11 and EDB, (d) dye-B1 and Iod, (e) dye-B10 and Iod, (f) dye-B11 and Iod in  
 425 dichloromethane.

426

427 4. **Table 4.** Parameters of the chemical mechanisms associated with B1, B3, B10,  
 428 B12 and B16 in dichloromethane.

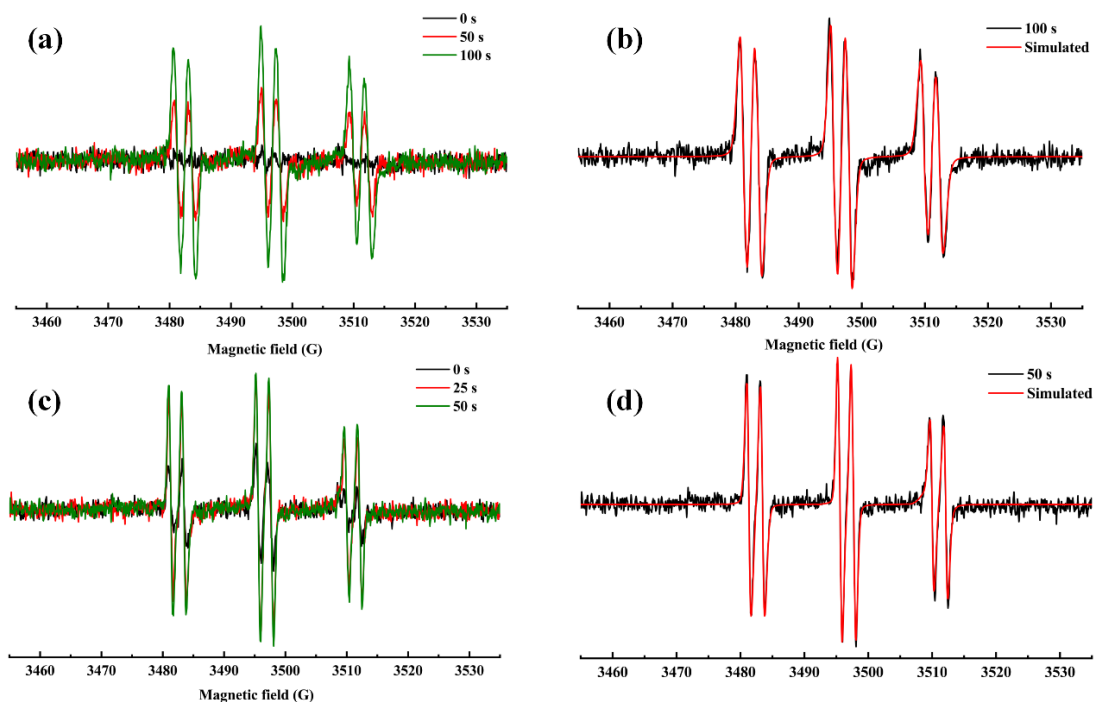
	<b>Dye-B1</b>	<b>Dye-B3</b>	<b>Dye-B10</b>	<b>Dye-B12</b>	<b>Dye-B16</b>
$E_{ox}$ (V)	-	0.83	-	-	1.02
$E_{red}$ (V)	-0.85	-1.09	-1.12	-1.04	-1.23
$\Delta G_{EDB}^{S1}$ (eV)	-0.64	-0.55	-0.51	-0.55	-0.06
$\Delta G_{Iod}^{S1}$ (eV)	-	-1.11	-	-	-0.45
$E_{S1}$ (eV)	2.49	2.64	2.63	2.59	2.29
$K_{sv}$ (EDB) $s^{-1}$	43.9	19.1	58.4	91.3	-
$K_{sv}$ (Iod) $s^{-1}$	24.7	23.5	17.2	34.6	18.9
$\phi_{et}$ (EDB) <sup>a</sup>	0.69	0.49	0.74	0.82	-
$\phi_{et}$ (Iod) <sup>a</sup>	0.33	0.32	0.26	0.41	0.27

429 a : the electron transfer quantum yield is calculated from:  $\phi_{et} = K_{sv} [additive] / (1 + K_{sv} [additive])$ ;  
 430 with [additive] the EDB (0.05 M) and Iod (0.02 M) concentration.

431

#### 432 **4.1 ESR-ST experiments.**

433 To determine the nature of the free radicals produced by the interaction between  
 434 dye/EDB and dye/Iod, B1 was used as an example to successfully carry out ESR-ST  
 435 experiments under the LED@405 nm (See Figure 8). As shown in Figures 8 (a) and (b),  
 436 for the dye/EDB system, a free radical was successfully captured by PBN, and its  
 437 hyperfine coupling constants were  $\alpha_N = 14.3$  G and  $\alpha_H = 2.6$  G, which may be  
 438 aminoalkyl radical  $EDB_{(-H)}\cdot$ . In Figures 8 (c) and (d), a radical in the dye/Iod system  
 439 was captured by PBN, and its hyperfine coupling constants were  $\alpha_N = 14.3$  G and  $\alpha_H$   
 440  $= 2.2$  G, which may be aryl radical. The results are in accordance with the experimental  
 441 data reported in the literature [31].



442

443 **Figure 8.** ESR-ST spectra of the PBN radical adducts (in *tert*-butylbenzene under  
 444 nitrogen atmosphere). (a) and (b) B1/EDB, (c) and (d) B1/Iod under LED@405 nm  
 445 irradiation.

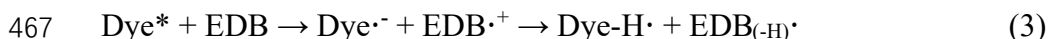
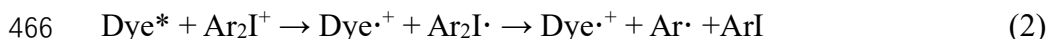
446

#### 447 **4.2 Summary of photoinitiation mechanisms of dye.**

448 Based on the above results, the chemical mechanisms induced by the three-  
 449 component photoinitiating dye/EDB/Iod system was proposed, which can be divided  
 450 into three steps. The first step consisted in the excitation of the chromophore with light,  
 451 enabling to promote the dye from its initial ground state to the excited state (See  
 452 reaction 1). In the second step, the excited dye\* reacted with Iod and EDB respectively  
 453 to generate free radicals, as shown in reactions 2 and 3. Specifically, the dye\* reacted  
 454 with Iod to generate Ar· free radicals and dye·<sup>+</sup>. In addition, dye\* reacted with EDB to  
 455 produce EDB<sub>(-H)</sub>· free radicals and dye-H·. In fact, the excited dye (dye\*) can react with  
 456 EDB and Iod separately according to a reductive and an oxidative pathway so that free  
 457 radicals capable of initiating polymerization processes were produced. In a third step,  
 458 Dye·<sup>+</sup> produced by an oxidation reaction and Dye-H· produced by a reduction reaction  
 459 can be regenerated into Dye by the interaction with EDB and Iod respectively (See  
 460 reactions 4 and 5), and finally the catalytic cycle of the three-component system was

461 completed. Notably, the free radicals  $\text{EDB}_{(-\text{H})}\cdot$  and  $\text{Ar}\cdot$  produced during the catalytic  
462 cycle were successfully detected by ESR, which provided clear evidences for the  
463 proposed chemical mechanisms.

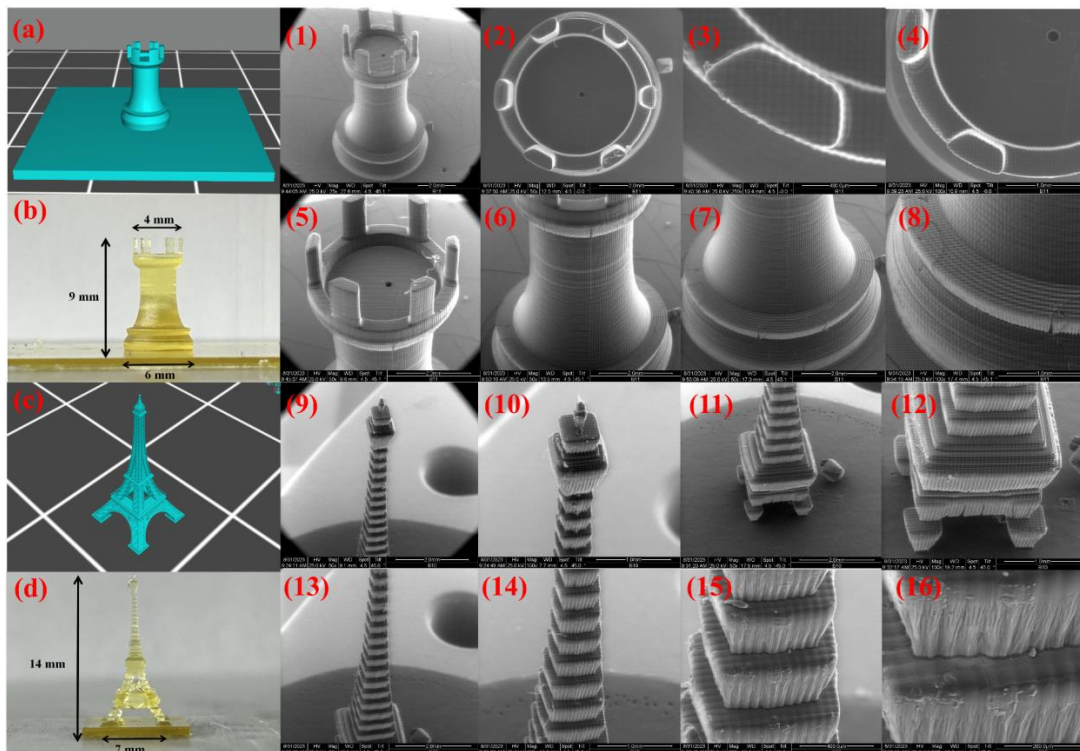
464



470

### 471 **4.3 Application in 3D printing**

472 Exploiting the impressive photoinitiation capabilities demonstrated by several  
473 dyes in this study (efficiently initiate the FRP of TMPTA under both of LED@405 nm  
474 irradiation and exposure to sunlight) we selected the two-component systems B3/EDB,  
475 B10/EDB, and B12/EDB, along with the three-component systems B10/EDB/Iod and  
476 B11/EDB/Iod for 3D printing. For the DLW experiments, the two-component systems  
477 were employed, resulting in the rapid production of 3D letters within 2 min of  
478 irradiation at 405 nm, as depicted in Figure S23. These outcomes were verified through  
479 digital camera and numerical optical microscopy, highlighting the distinct and well-  
480 defined outlines of printed letters. Moving to the 3D printing experiment involving the  
481 three-component system, Figure 9 illustrates the successful printing of an exquisite  
482 chess piece and an Eiffel tower model using a 3D printer Figures 9 (a) and (b) depict  
483 the chess piece model printed by B11/EDB/Iod/TMPTA system, and Figures 9 (c) and  
484 (d) showcase the Eiffel tower model printed by B10/EDB/Iod/TMPTA system. The  
485 clear outline of the model is readily discernible through digital camera observation, and  
486 SEM photos (See Figure 9 (1-16)) further confirm the smooth surfaces and excellent  
487 spatial resolution achieved in the production of these 3D objects. These results  
488 underscore the potential of the selected photoinitiating systems for high-quality and  
489 precise 3D printing applications.



490

491 **Figure 9.** Digital photos of 3D printed objects. (a) and (b) dye-  
 492 B11(0.1wt%)/EDB(1wt%)/Iod(1wt%)/TMPTA system; (c) and (d) dye-  
 493 B10(0.1wt%)/EDB(1wt%)/Iod(1wt%)/TMPTA system; 1-8 SEM images of surface of  
 494 the 3D printed objects using dye-B11/EDB/Iod/TMPTA system; 9-16 SEM images of  
 495 surface of the 3D printed objects using dye-B10/EDB/Iod/TMPTA system.

496

#### 497 **4.4 Comparisons with solar photoinitiators from previous studies**

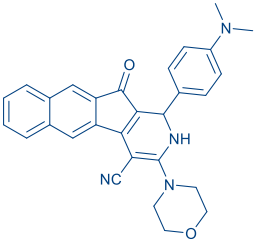
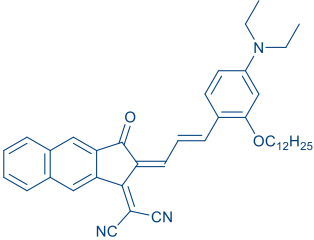
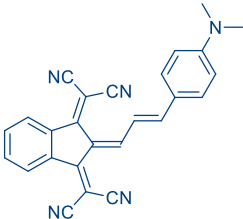
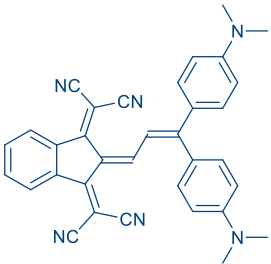
498 In Figure 4, photopolymerization profiles obtained with B1, B2, B3, B10, and B11  
 499 upon sunlight irradiation in two- and three-component photoinitiating systems are  
 500 presented. A thorough comparison with dyes previously reported in the literature  
 501 accentuates the remarkable performance of the dyes investigated in this study. Table 5  
 502 outlines the superior attributes of the identified top candidates for the FRP of TMPTA  
 503 in the literature, where all polymerization experiments utilized a three-component  
 504 dye/EDB/Iod system with concentrations set at 0.1%/2%/2% w/w/w. In contrast to prior  
 505 experiments, our approach exhibited a substantial 20-fold reduction in the  
 506 concentration of additives while maintaining a high monomer conversion.  
 507 Simultaneously, the exposure time to sunlight was significantly curtailed, achieving



508 remarkable monomer conversions within just 70 s of sunlight irradiation, as opposed to  
 509 the to 30 min required in earlier studies. In light of these findings and to the best of our  
 510 knowledge [32, 33], B1, B2, B3, B10, and B11 represent the inaugural sunlight  
 511 photoinitiators capable of utilizing additives at such minimal concentrations,  
 512 concurrently achieving high monomer conversions within approximately one minute of  
 513 sunlight exposure. This advancement positions these dyes at the forefront of solar  
 514 photoinitiators in terms of efficiency and expeditious polymerization under sunlight.

515

516 **Table 5.** Acrylate function conversions obtained during the FRP of TMPTA at 405 nm  
 517 and sunlight (30 min) using three-component photoinitiating dye/Iod/EDB (0.1%/2%/2%  
 518 w/w/w) systems.

	Push-pull dyes	Absorption properties	Final Acrylate function conversion
Dye8 [34]		$\lambda_{\max} = 491 \text{ nm}$ $\epsilon_{\max} = 5330 \text{ M}^{-1} \cdot \text{cm}^{-1}$ $\epsilon_{405\text{nm}} = 3340 \text{ M}^{-1} \cdot \text{cm}^{-1}$	~91% (LED@405 nm, I = 110 mW.cm <sup>-2</sup> , 400 s); ~88% (sunlight, 30 min)
CP7 [35]		$\lambda_{\max} = 689 \text{ nm}$ $\epsilon_{\max} = 113870 \text{ M}^{-1} \cdot \text{cm}^{-1}$ $\epsilon_{405\text{nm}} = 13640 \text{ M}^{-1} \cdot \text{cm}^{-1}$	~97% (LED@405 nm, I = 30 mW.cm <sup>-2</sup> , 400 s); ~93% (sunlight, 30 min)
CP9 [35]		$\lambda_{\max} = 627 \text{ nm}$ $\epsilon_{\max} = 51700 \text{ M}^{-1} \cdot \text{cm}^{-1}$ $\epsilon_{405\text{nm}} = 4610 \text{ M}^{-1} \cdot \text{cm}^{-1}$	~98% (LED@405 nm, I = 30 mW.cm <sup>-2</sup> , 400 s); ~91% (sunlight, 30 min)
CP11 [35]		$\lambda_{\max} = 671 \text{ nm}$ $\epsilon_{\max} = 47770 \text{ M}^{-1} \cdot \text{cm}^{-1}$ $\epsilon_{405\text{nm}} = 6560 \text{ M}^{-1} \cdot \text{cm}^{-1}$	~99% (LED@405 nm, I = 30 mW.cm <sup>-2</sup> , 400 s); ~92% (sunlight, 30 min)

## 519 **5. Conclusion**

520 In this study, we synthesized and explored the potential of 15 new dyes based on  
521 the 2-phenylnaphtho[2,3-*d*]thiazole-4,9-dione scaffold and 1 dye based on the 2,3-  
522 diphenyl-1,2,3,4-tetrahydrobenzo[*g*]quinoxaline-5,10-dione scaffold as photoinitiators.  
523 All dyes examined in this work have never previously been studied as photosensitizers  
524 for photopolymerization processes. Particularly noteworthy is the fact that, despite the  
525 synthesis of 2,3-diphenyl-1,2,3,4-tetrahydrobenzo[*g*]quinoxaline-5,10-diones being  
526 reported in 1987, subsequent investigations into this family of dyes have been notably  
527 sparse. Diverse photoinitiating systems were prepared by combining these dyes with  
528 additives such as EDB and Iod. The strong absorption of these dyes exhibited in the  
529 UV-visible region ( $> 400$  nm) facilitated photopolymerization under the irradiation of  
530 LED@405 nm and LED@450 nm. The proposed chemical mechanism was  
531 corroborated using complementary techniques including steady-state photolysis,  
532 fluorescence quenching experiments, cyclic voltammetry, and ESR-ST experiments.  
533 Remarkably, B1, B2, B3, B10, and B11 emerged as successful photoinitiators for the  
534 FRP of TMPTA under sunlight due to their excellent photoinitiation ability. Among  
535 these, B10 exhibited the highest reactivity, achieving unprecedented monomer  
536 conversions under sunlight, with FCs of 58% for TMPTA and 96% for PEGDA, all at  
537 significantly low concentrations of photosensitizers and additives. These findings  
538 position these dyes as promising candidates for the future development of efficient  
539 sunlight photoinitiators. Finally, the three-component systems, B10/EDB/Iod and  
540 B11/EDB/Iod, were successfully applied to 3D printing. In summary, the demonstrated  
541 ability of these dyes to initiate polymerization under sunlight, coupled with their ease  
542 of synthesis, rapid polymerization under both sunlight and artificial light sources, aligns  
543 with the principles of green chemistry. These chromophores present a viable option for  
544 large-scale industrial applications, such as exterior wall coatings, offering energy  
545 efficiency and environmental sustainability in outdoor polymerization processes.

546

547

548 **Conflicts of interest**

549 The authors declare no competing financial interest.

550

551 **Acknowledgements**

552 This research project is supported by China Scholarship Council (CSC)

553 (No.202208220049).

554

555 **References**

- 556 1. Kaur; Manmeet; Srivastava; A.; K., *Journal of Macromolecular Science: Polymer*  
557 *Reviews* **2002**, *42* (4), 481-481.
- 558 2. Corrigan, N.; Yeow, J.; Judzewitsch, P.; Xu, J.; Boyer, C., *Angew Chem Int Ed*  
559 *Engl* **2019**, *58* (16), 5170-5189. DOI 10.1002/anie.201805473.
- 560 3. Zhang, Y.; Liu, Z.; Borjigin, T.; Graff, B.; Morlet-Savary, F.; Schmitt, M.; Gignes,  
561 D.; Dumur, F.; Lalevée, J., *Green Chemistry* **2023**, *25* (17), 6881-6891. DOI  
562 10.1039/d3gc02004e.
- 563 4. Mokbel, H.; Graff, B.; Dumur, F.; Lalevee, J., *Macromol Rapid Commun* **2020**, *41*  
564 (15), e2000289. DOI 10.1002/marc.202000289.
- 565 5. Weems, A. C.; Delle Chiaie, K. R.; Yee, R.; Dove, A. P., *Biomacromolecules* **2020**,  
566 *21* (1), 163-170. DOI 10.1021/acs.biomac.9b01125.
- 567 6. Zhou, A.; Xu, C.; Kanitthamniyom, P.; Ng, C. S. X.; Lim, G. J.; Lew, W. S.; Vasoo,  
568 S.; Zhang, X.; Lum, G. Z.; Zhang, Y., *Adv Mater* **2022**, *34* (15), e2200061. DOI  
569 10.1002/adma.202200061.
- 570 7. Khudyakov, I. V., *Progress in Organic Coatings* **2018**, *121*, 151-159. DOI  
571 10.1016/j.porgcoat.2018.04.030.
- 572 8. Wang, S.-C.; Wu, Y.-H.; Hsieh, J.-B.; Ni, J.-S.; Chen, Y.-C., *Journal of*  
573 *Photochemistry and Photobiology A: Chemistry* **2023**, *443*. DOI  
574 10.1016/j.jphotochem.2023.114870.
- 575 9. Chen, L.; Kenkel, S. M.; Hsieh, P. H.; Gryka, M. C.; Bhargava, R., *ACS Appl*  
576 *Mater Interfaces* **2020**, *12* (44), 50105-50112. DOI 10.1021/acsami.0c12158.
- 577 10. Abedin, F.; Ye, Q.; Spencer, P., *J Dent* **2020**, *99*, 103405. DOI  
578 10.1016/j.jdent.2020.103405.
- 579 11. Xue, T.; Tang, L.; Tang, R.; Li, Y.; Nie, J.; Zhu, X., *Dyes and Pigments* **2021**, *188*.  
580 DOI 10.1016/j.dyepig.2021.109212.
- 581 12. Fang, W. W.; Yang, G. Y.; Fan, Z. H.; Chen, Z. C.; Hu, X. L.; Zhan, Z.; Hussain,  
582 I.; Lu, Y.; He, T.; Tan, B. E., *Nat Commun* **2023**, *14* (1), 2891. DOI  
583 10.1038/s41467-023-38402-y.

- 584 13. Voll, D.; Barner-Kowollik, C., *Angewandte Chemie International Edition* **2013**,  
585 52 (12), 3312-3312. DOI 10.1002/anie.201209688.
- 586 14. Liao, W.; Liao, Q.; Xiong, Y.; Li, Z.; Tang, H., *Journal of Photochemistry and*  
587 *Photobiology A: Chemistry* **2023**, 435. DOI 10.1016/j.jphotochem.2022.114297.
- 588 15. Lee, Y.; Boyer, C.; Kwon, M. S., *Nature Reviews Materials* **2021**, 7 (2), 74-75.  
589 DOI 10.1038/s41578-021-00409-6.
- 590 16. Fast, D. E.; Lauer, A.; Menzel, J. P.; Kelterer, A.-M.; Gescheidt, G.; Barner-  
591 Kowollik, C., *Macromolecules* **2017**, 50 (5), 1815-1823. DOI  
592 10.1021/acs.macromol.7b00089.
- 593 17. Li, J.; Zheng, H.; Lu, H.; Li, J.; Yao, L.; Wang, Y.; Zhou, X.; Nie, J.; Zhu, X.; Fu,  
594 Z., *European Polymer Journal* **2022**, 176. DOI 10.1016/j.eurpolymj.2022.111393.
- 595 18. Bella, F.; Sacco, A.; Salvador, G. P.; Bianco, S.; Tresso, E.; Pirri, C. F.;  
596 Bongiovanni, R., *The Journal of Physical Chemistry C* **2013**, 117 (40), 20421-  
597 20430. DOI 10.1021/jp405363x.
- 598 19. Ye, S.; Shi, W.; Liu, Y.; Li, D.; Yin, H.; Chi, H.; Luo, Y.; Ta, N.; Fan, F.; Wang, X.;  
599 Li, C., *J Am Chem Soc* **2021**, 143 (32), 12499-12508. DOI 10.1021/jacs.1c00802.
- 600 20. Winther-Jensen, O.; Armel, V.; Forsyth, M.; MacFarlane, D. R., *Macromolecular*  
601 *Rapid Communications* **2010**, 31 (5), 479-483. DOI 10.1002/marc.200900701.
- 602 21. Zhao, Y.; Ding, C.; Zhu, J.; Qin, W.; Tao, X.; Fan, F.; Li, R.; Li, C., *Angew Chem*  
603 *Int Ed Engl* **2020**, 59 (24), 9653-9658. DOI 10.1002/anie.202001438.
- 604 22. Schmitt, M., *Nanoscale* **2015**, 7 (21), 9532-44. DOI 10.1039/c5nr00850f.
- 605 23. Hammoud, F.; Hijazi, A.; Duval, S.; Lalevee, J.; Dumur, F., *European Polymer*  
606 *Journal* **2022**, (162-), 162.
- 607 24. Mokbel, H.; Noirbent, G.; Gimes, D.; Dumur, F.; Lalevee, J., *Beilstein J Org*  
608 *Chem* **2021**, 17, 2067-2076. DOI 10.3762/bjoc.17.133.
- 609 25. Abdallah, M.; Dumur, F.; Graff, B.; Hijazi, A.; Lalevée, J., *Dyes and Pigments*  
610 **2020**, 182. DOI 10.1016/j.dyepig.2020.108580.
- 611 26. Fouassier; JeanPierre, *Wiley-VCH* **2012**.
- 612 27. Romańczyk, P. P.; Kurek, S. S., *Electrochimica Acta* **2017**, 255, 482-485.

- 613 28. Yu, Z.; Su, J.; Huang, C.; Wei, J.; Han, L.; Ye, Q.; Li, Y., *Asian Journal of Organic*  
614 *Chemistry* **2022**.
- 615 29. Haug, J.; Scheffler, K.; Stegmann, H. B.; Vonwirth, S.; Wei, J. E.; Conzelmann,  
616 W.; Hiller, W., *European Journal of Inorganic Chemistry* **1987**, 120 (7), 1125-1132.
- 617 30. Han, W.; Shi, Y.; Xue, T.; Wang, T., *Dyes and Pigments* **2019**, 166, 140-148. DOI  
618 10.1016/j.dyepig.2019.03.023.
- 619 31. Lalevée, J.; Gigmes, D.; Bertin, D.; Graff, B.; Allonas, X.; Fouassier, J. P.,  
620 *Chemical Physics Letters* **2007**, 438 (4-6), 346-350. DOI  
621 10.1016/j.cplett.2007.03.029.
- 622 32. Tehfe, M.; Louradour, F.; Lalevée, J.; Fouassier, J.-P., *Applied Sciences* **2013**, 3  
623 (2), 490-514. DOI 10.3390/app3020490.
- 624 33. Dumur, F., *Eur. Polym. J.* **2023**, 189, 111988-112008.
- 625 34. Sun, K.; Liu, S.; Pigot, C.; Brunel, D.; Graff, B.; Nechab, M.; Gigmes, D.; Morlet-  
626 Savary, F.; Zhang, Y.; Xiao, P.; Dumur, F.; Lalevée, J., *Catalysts* **2020**, 10 (10).  
627 DOI 10.3390/catal10101196.
- 628 35. Sun, K.; Pigot, C.; Zhang, Y.; Borjigin, T.; Morlet-Savary, F.; Graff, B.; Nechab,  
629 M.; Xiao, P.; Dumur, F.; Lalevée, J., *Macromolecular chemistry and physics* **2022**,  
630 (4), 223.
- 631